

RESEARCH ARTICLE

10.1002/2014JB011859

A new seismically constrained subduction interface model for Central America

C. Kyriakopoulos^{1,2}, A. V. Newman¹, A. M. Thomas³, M. Moore-Driskell⁴, and G. T. Farmer¹

Key Points:

- New 3-D model for the plate interface along the Middle America Trench
- The model interface captures local features not seen in other models
- Interface heterogeneity associated with seafloor subduction

Supporting Information:

- Supporting Information S1
- Figure S1
- Figure S2

Correspondence to:

C. Kyriakopoulos,
christos@ucr.edu

Citation:

Kyriakopoulos, C., A. V. Newman, A. M. Thomas, M. Moore-Driskell, and G. T. Farmer (2015), A new seismically constrained subduction interface model for Central America, *J. Geophys. Res. Solid Earth*, 120, doi:10.1002/2014JB011859.

Received 24 DEC 2014

Accepted 1 JUL 2015

Accepted article online 14 JUL 2015

¹School of Earth and Atmospheric Sciences, Georgia Institute of Technology, Atlanta, Georgia, USA, ²Now at Department of Earth Sciences, University of California, Riverside, California, USA, ³Department of Geological Sciences, University of Oregon, Eugene, Oregon, USA, ⁴Department of Physics and Earth Science, University of North Alabama, Florence, Alabama, USA

Abstract We provide a detailed, seismically defined three-dimensional model for the subducting plate interface along the Middle America Trench between northern Nicaragua and southern Costa Rica. The model uses data from a weighted catalog of about 30,000 earthquake hypocenters compiled from nine catalogs to constrain the interface through a process we term the “maximum seismicity method.” The method determines the average position of the largest cluster of microseismicity beneath an a priori functional surface above the interface. This technique is applied to all seismicity above 40 km depth, the approximate intersection of the hanging wall Mohorovičić discontinuity, where seismicity likely lies along the plate interface. Below this depth, an envelope above 90% of seismicity approximates the slab surface. Because of station proximity to the interface, this model provides highest precision along the interface beneath the Nicoya Peninsula of Costa Rica, an area where marked geometric changes coincide with crustal transitions and topography observed seaward of the trench. The new interface is useful for a number of geophysical studies that aim to understand subduction zone earthquake behavior and geodynamic and tectonic development of convergent plate boundaries.

1. Introduction

Convergent tectonic boundaries are responsible for the release of more than 80% of the globally observed seismic moment [Pacheco and Sykes, 1992], primarily occurring along the subduction interface, termed the megathrust. These megathrust events are a severe threat to populations living near the coast. The danger is a result of both the generated strong shaking and triggering tsunami waves leading, in the worst case scenario, to the total destruction of coastal communities. Thus, it is important to understand the physical factors controlling the seismic potential and accumulation of elastic energy along subduction zones. The Middle America Trench (MAT) dominates the oceanic landscape of the southwestern coast of Central America. In this actively deforming region the Cocos and Caribbean Plates converge rapidly at a rate of approximately 8–9 cm/yr [DeMets *et al.*, 2010]. As the two plates move toward one another, the Cocos Plate subducts beneath the overriding Caribbean Plate. The most tangible effect of this subduction is the generation of large thrust earthquakes such as the moment magnitude (M_w) 7.6 1992 Nicaraguan tsunami earthquake [Kikuchi and Kanamori, 1995] or the most recent M_w 7.6 Nicoya 2012 earthquake, which occurred almost entirely under the peninsula of Nicoya [Protti *et al.*, 2014]. In particular, this is a region where extensive multidisciplinary studies (e.g., seismic experiments, geodetic campaigns, hydrogeological studies, and detailed bathymetric mapping) have been conducted in the last 20 years, including an ongoing dense seismic and geodetic network in the Nicoya Peninsula, termed the Nicoya Seismic Cycle Observatory (NSCO).

The material composition of the subducting Cocos Plate has two origins, the East Pacific Rise (EPR) crust in the north and the Cocos-Nazca Spreading Center (CNS) crust in the south [Barckhausen *et al.*, 2001]. Previous seismological studies revealed that transition from EPR to CNS crust coincides with an abrupt 5 km reduction in depth in the interface microseismicity, possibly related to an abrupt change of the interface geometry [Newman *et al.*, 2002; DeShon *et al.*, 2006], and a net change in the thermal state of the incoming plate [Harris *et al.*, 2010]. Simulations of earthquake dynamic rupture implementing nonplanar faults demonstrated that interface geometry plays a controlling role in rupture propagation [e.g., Duan and Oglesby, 2005; Yang *et al.*, 2013]. However, existing interseismic locking [Feng *et al.*, 2012] and coseismic slip models [Yue *et al.*, 2013; Protti *et al.*, 2014] of the Costa Rica subduction zone are based on smoothed

and regionally averaged subduction fault geometry, ignoring the along-strike variation of the subduction interface from EPR to CNS. The inclusion of such geometric changes are likely to have a significant effect on the distribution of locking and moment release predicted from models of interseismic and coseismic deformation in the area, which already show that both peak locking and slip occur right at the transition between EPR and CNS crust.

A number of studies have focused on creating three-dimensional (3-D) models of subduction zone geometries, with results dependent upon the data and methods used. Models are driven by observations of local or teleseismically observed earthquake activity, regional seismic profiling, tomography, or some combination of these. Globally, *Gudmundsson and Sambridge* [1998] proposed a three-dimensional model of subducting slabs, useful for improved teleseismic earthquake locations when accounting for perturbations in seismic velocities in the mantle. *Syracuse and Abers* [2006] proposed an updated global model of subduction zone geometries using a combination of teleseismic and local seismicity. While these models are good representations of the subducted slabs, they lack resolution of the subduction megathrust interface responsible for the generation of potentially devastating earthquakes. However, the work of *Hayes et al.* [2012] aimed to rectify this for about 85% of global subduction zones in a model called Slab1.0. This study combines numerous independent observations, including historic earthquake catalogs, relocated teleseismic events, bathymetry, sediment thickness, and active source seismic data.

Regionally, a few locally derived 3-D interfaces have been created [*Protti et al.*, 1994; *Ranero et al.*, 2005, *DeShon et al.*, 2006]. Similar to the global models results, these results depend upon data, method, and depth of investigation. A systematic analysis of the variations of the Wadati-Beniof zone beneath Nicaragua and Costa Rica was the focus of *Protti et al.* [1994], in which they concluded that abrupt changes of the zone beneath Nicaragua and Costa Rica correspond with along-trench variations of the age of the subducting Cocos Plate. In a study that focused on the relationship between plate-bending faults along subduction zones in both Chile and Central America, *Ranero et al.* [2005] developed a pair of new slab models based on a combination of global seismic tomography, and teleseismic and regional earthquake locations. In developing a new locally derived seismic velocity model for the Nicoya Peninsula, *DeShon et al.* [2006] also illuminated some of the along-strike changes of the megathrust that correspond to the EPR-CNS transition first identified by *Newman et al.* [2002]. Finally, hypocenter locations and seismic tomography were used by *Syracuse et al.* [2008] to determine the slab geometry with the specific goal of understanding geochemical variations and their association with the slab thickness beneath Central America. Because of the project goals and network design, the Syracuse study best described the geometry away from the megathrust interface and below the volcanic chain.

For a number of geophysical studies, accurate information about details of the subducting plate interface is important. A fundamental component of the geodetic modeling of subduction zones is the correct prediction of surface displacements generated by slip along the fault interface. In order to better understand the mechanisms controlling the accumulation of interseismic elastic energy, and subsequently the release of the seismic energy during the coseismic phase, it is important to define the characteristics of the fault interface. The development of accurate subduction interface models is critical in geodetic modeling and more precisely in estimating the interseismic locking map, coseismic slip distribution, slow slip events, seafloor displacement useful for tsunami wave simulations, and dynamic rupture scenarios. In this work we present a high-resolution MAT subduction fault interface model generated from hypocenters of small earthquakes recorded from several seismic networks across the interface offshore and beneath Costa Rica and Nicaragua.

2. Earthquake Catalogs

Our composite seismic catalog comprises events recorded by eight seismic networks along Costa Rica and Nicaragua. These networks include data recorded along Costa Rica as part of the Costa Rica Seismogenic Zone Experiment, along central Costa Rica and Nicaragua as part of the German SFB 574 program, across Nicaragua from the Nicaraguan national network, and across both regions during the Tomography Under Costa Rica and Nicaragua (TUCAN) experiment (Figure 1a). Additionally, the JACO and QUEPOS experiments (part of SFB574) provide coverage for the offshore region between the Nicoya and Osa Peninsulas. The data from these networks allow for approximately 700 km of trench parallel coverage

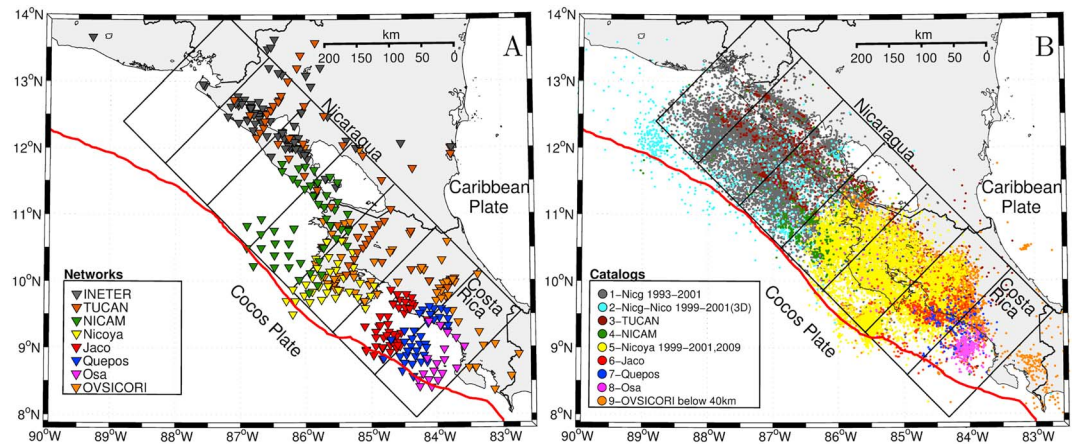


Figure 1. Seismic networks and microseismicity. (a) The networks are the Seismic Network of Nicaragua (SNN)—INETER permanent network, the TUCAN temporary array, the NICAM SFB574 experiment, the Nicoya and Osa CRSEIZE temporary arrays, the Jaco temporary array, the Quepos temporary array, and the Observatorio Vulcanológico y Sismológico de Costa Rica, Universidad Nacional (OVSICORI) network. (b) Regional microseismicity color coded by the local network in which they were recorded (see Figure 1a). The bathymetric low defining the Middle America Trench is traced in red.

along the Wadati-Benioff seismic zone (Figure 1b). Details of the individual networks and their resultant hypocenter catalogs are presented in the following sections in the order of descending latitudinal position. For catalogs in which we had seismic phase information, we relocated the events using one of two locally available velocity models, as described in the following sections. Summing the events from these catalogs, we use about 30,000 earthquakes occurring between 1993 and 2009. The spatial coverage of each data set is represented jointly with the deployed seismic networks in Figure 1.

2.1. Nicaragua INETER 1993–2001

The Seismic Network of Nicaragua (SNN) operated by the Instituto Nicaraguense de Estudios Territoriales (INETER) recorded earthquake activity that best describes the subduction geometry offshore the Nicaraguan coast for the time period from 1993 to 2001 (catalog 1 in Figure 1b). The network operates 37 telemetered seismic short period and 15 broadband stations distributed across Nicaragua. The data set is composed of about 11,300 events which we relocated using SimulPS [Thurber, 1983, 1993; Eberhart-Phillips, 1990; Evans et al., 1994] within a two-dimensional V_p and V_p/V_s velocity model extrapolated northward from northern Costa Rica, a region with comparable plate geometry and crustal origins [DeShon et al., 2006]. The events have formal position errors of 1.79, 1.12, and 2.63 km (hereafter errors are reported in longitude, latitude, and depth positions, respectively).

2.2. Nicaragua-Nicoya 1999–2001 (3-D)

For events that were located both by the Nicaraguan national network (section 2.1) and the Nicoya-CRSEIZE network (section 2.5), a new combined catalog was developed from cross-network detection of events (catalog 2 in Figure 1b). These events are reported for the period in which the Nicoya-CRSEIZE network was operational, from late 1999 to middle 2001. The new catalog of 893 earthquakes was created from the two independent catalogs of P and S phase arrivals, merging events when temporal differences in earthquake origin times were less than 10 s. The events, with formal position errors of 0.79, 0.48, and 0.94 km, were located in the same velocity model as the larger Nicaraguan-only catalog describe in section 2.1. The unique positioning of the combination of the Nicoya-CRSEIZE and SNN networks allowed for detailed imaging of seismic events offshore of southern Nicaragua and northwest of the Nicoya Peninsula.

2.3. TUCAN Data Set

Syracuse et al. [2008] created a region-wide catalog of 1328 earthquakes primarily under the volcanic belts (catalog 3 in Figure 1b) from recording made during a large temporary deployment called the TUCAN array (Tomography Under Costa Rica and Nicaragua). The array consisted of 47 broadband stations operating from July 2004 to March 2006. The distribution of the stations was mainly organized in four

trench-normal lines from northern Nicaragua to central Costa Rica. The data were collected and processed by a joint group from the Observatorio Vulcanológico y Sismológico de Costa Rica, Universidad Nacional (OVSICORI) of the National University of Costa Rica, INETER, and Boston University. Because of the location and network design, these data are uniquely well suited for recording deep earthquakes along the deeper Wadati-Benioff zone but insufficient for characterizing the subduction megathrust through the region. Earthquakes were located within a regional velocity model also developed by *Syracuse et al.* [2008] and have average formal errors of 1.77, 1.47, and 2.35 km.

2.4. Nicaragua Amphibious Data Set (SFB-574 Project)

The Nicaragua amphibious (SFB 574 project) data set consists of 582 events, hereafter the NICAM catalog (catalog 4 in Figure 1b). The original data set was acquired from a temporary network of offshore ocean bottom seismometers (OBS), ocean bottom hydrophones (OBH), and temporary short-period land stations. The array was deployed for a total of 6 months between December 2005 and June 2006. The experiment was conducted by the Christian Albrechts University of Kiel and the former Leibniz Institute of Marine Sciences at the University of Kiel (IFM-GEOMAR). We relocated these events using TomoDD in a region-wide 3-D V_p and V_s velocity models by *Moore-Driskell et al.* [2013].

For this catalog, as well as the Nicoya (section 2.5), JACO and Quepos (section 2.6), and Osa (section 2.7) catalogs, we performed jackknife analyses of the solution variability by systematically excluding one station at a time while determining event locations across the catalog. Because any one event is only located by a subset of the network, most solutions are near identical to the original and only vary substantially when one of the stations used in that individual event is removed. Because of this, we considered the range of solutions to contain approximately 95% of likely results; thus, we report errors of one quarter the overall range; corresponding to one standard deviation of a Gaussian distribution. For the NICAM catalog we obtain jackknife errors of 350, 340, and 415 m.

2.5. Nicoya 1999–2001 (CRSEIZE), 2009

The Costa Rica Seismogenic Zone Experiment (CRSEIZE) was a combined seismic and geodetic project operated by University of California (UC) Santa Cruz, UC San Diego, OVSICORI, and the University of Miami, to image the seismogenic plate interface offshore the Nicoya and Osa Peninsulas of Costa Rica. The CRSEIZE network was composed of 20 three-component short-period and broadband seismometers on the Nicoya peninsula as well as 14 broadband ocean bottom seismometers [*Newman et al.*, 2002]. The observations derived from these experiments provide a unique opportunity to evaluate the main seismogenic interface that is responsible for the region's largest earthquakes. In Nicoya, the land-based component of the experiment operated from December 1999 to June 2001 while the offshore segment was operated from December 1999 to June 2000. The total data set is composed of 11,241 events with average jackknife errors of 75, 81, and 115 m (catalog 5 in Figure 1b). The 2009 catalog is a data set recorded by an ongoing seismic network reoccupying most of the same sites as the original Nicoya-CRSEIZE on land deployment. The new network, reinitiated in 2008, was operated jointly by UC Santa Cruz, Georgia Institute of Technology, and OVSICORI and is part of the NSCO. While the network is still ongoing at the time of this writing, the 2009 data set, which is composed entirely of analyst phase picks, was considered to be sufficiently representative in terms of geometry of hypocenter locations, particularly when added to the existing Nicoya-CRSEIZE data set. We relocate both data sets within the TomoDD V_p and V_s velocity models of *Moore-Driskell et al.* [2013].

2.6. JACO and QUEPOS Data Set (SFB574 Project)

The Jaco (JACO) and Quepos (QUEPOS) Costa Rica experiments, named after coastal towns, are two amphibious seismological networks deployed between the Nicoya and Osa Peninsulas from April 2002 to October 2002 and from September 2002 to May 2003, respectively [*Arroyo et al.*, 2009; *Dinc et al.*, 2010]. The experiments were conducted with 10 ocean bottom seismometers (OBS), 13 ocean bottom hydrophones (OBH), and 15 on-land stations. The Jaco experiment was subsequently shifted 60 km south to become the Quepos experiment in 2003. These data were located using TomoDD in a region-wide 3-D V_p and V_s velocity model by *Moore-Driskell et al.* [2013], resulting in 1031 events from the JACO experiment and 298 events from the Quepos data set (catalogs 6 and 7 in Figure 1b), with average jackknife errors of

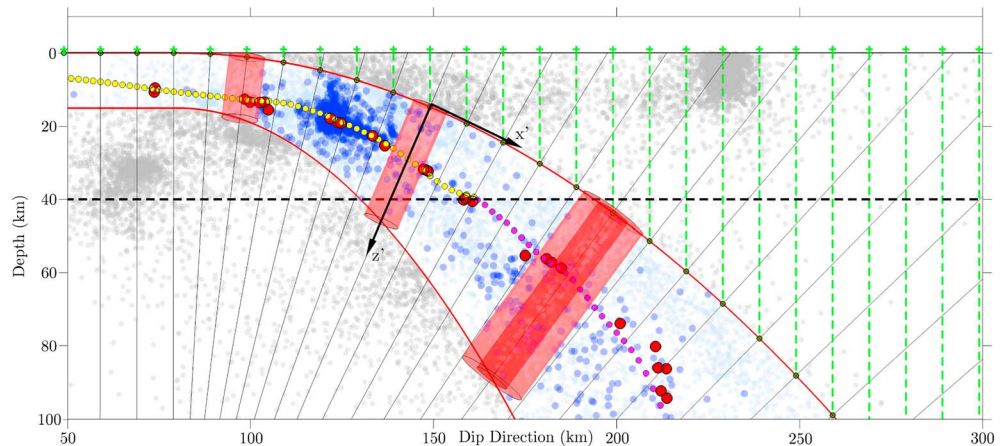


Figure 2. Schematic representation of the maximum seismicity method. The bounding initial parabolic functions (red curves) delimit near-slab seismicity (cyan circles), excluding outside events (gray circles). The green crosses represent the regular surface grid (for clarity we show 10 km steps) which are downward projected to the upper parabola (green dashed lines). Search cylinders (red) and an associated local r' - z' coordinate system (black arrows) are shown, with the local z' axis for each grid point shown as a thin gray line. The approximate depth of the Mohorovičić discontinuity (thick black dashed line) dictates a change in methodology used for the final determination. The final rough interface solutions per node (red circles) are shown relative to the final smoothed interface (solid yellow and magenta circles, color changing with method).

258, 256, and 325 m, and 60, 65, and 70 m, respectively. This experiment was also conducted by IFM-GEOMAR under the SFB574 project.

2.7. OSA CRSEIZE Data Set

The OSA deployment of the CRSEIZE experiment, named after the Osa Peninsula immediately to the south, recorded 2 months of aftershocks (mid-September through November) of the 20 August 1999 M_w 6.9 Quepos earthquake [DeShon *et al.*, 2003]. The seismic network was composed of 20 stations (6 onshore seismometers and 14 ocean bottom seismometers), recording 311 events (catalog 8 in Figure 1b). Like most of the above data sets, these were located using TomoDD in region-wide 3-D V_p and V_s velocity models by Moore-Driskell *et al.* [2013]. The average jackknife errors are 56, 46, and 72 m.

2.8. OVSICORI Data Set

Using the national seismic network maintained by OVSICORI, we obtained a catalog of 8768 earthquakes recorded between March 2010 and May 2014 and located using a regional 1-D velocity model within the Antelope seismic analysis software suite (www.brrt.com). Because these data represent a local composite catalog of events recorded using different methods, we filtered out possible duplicate events that had temporal separation of less than 5 s (removing 470 repeated records). These events are included as a secondary source for deep earthquakes below Costa Rica, supplementing the data from TUCAN, and thus, only events below 40 km depth are included. The final catalog consists of 2568 events with average formal errors of 229, 345, and 570 m.

3. Methodology

Because the earthquake data sets come from a number of sources with variable resolution, and because we are interested in developing a method that allows for spatially variable sensitivities from a distribution of networks, we developed a new tool for fault mapping. This tool, while specifically developed for this region, should be effective for other subduction zones, or otherwise seismically active faults. The method presented here, which we call the maximum seismicity method, is composed of eight basic steps, which are further explained below (Figure 2):

1. Perform initial filter to remove high error events in each catalog;
2. Remove known crustal events through the definition of an initial two-dimensional (2-D) confining function;
3. Define a gridded horizontal geometry over which to determine interface solutions;

4. For each grid point define a *minimum number of events* about a growing search radius normal to the upper surface of the confining initial function;
5. Apply a *sliding window* algorithm to identify maximum seismicity window for events within each grid node;
6. Weight individual events based on network location along-strike and their normalized errors within their catalog;
7. Solve for new three-dimensional (3-D) mean position for the interface based on the weighted average of event locations within the maximum seismicity window; and
8. Apply a resolution-based adaptive smoothing algorithm to create the final model.

The model is developed in a local coordinate system, 700 km in length and 250 km in width (Figure 1a) and oriented along the approximate strike of the Middle America Trench (45° counterclockwise (CCW) from the north and origin at longitude = -86.4° , latitude = 7°).

As an initial step, based on visual inspection of the scatter in earthquake locations we chose to remove 20% of the earthquakes with the highest 3-D hypocentral formal errors (sum of the mean errors in latitude, longitude, and depth) per catalog. This choice is somewhat subjective and may not be necessary if data are already filtered based on quality. From the remaining data, we manually define two a priori one-sided parabolic functions that vary in the along-dip direction and designed to confine subduction-related seismicity in order to avoid unnecessary bias from intraplate and volcanic seismicity, as well as other poorly located events below the downgoing plate (Figure 2). From this remaining data set, we perform an analysis across a 5×5 km regular grid oriented in the approximate along-strike and downdip directions. The grid spans a $700 \text{ km} \times 250 \text{ km}$ surface comprising 7191 investigated grid nodes. For each node, we evaluate the projection of the remaining seismicity within a cylinder normal to the top parabola. The search cylinder is initiated with a 5 km radius, about an axis z' , and grows by 1 km increments, until at least 25 earthquakes are retained. The 25-event minimum was chosen because test runs beneath Nicoya showed that at this value, solutions become robust and that larger values would unnecessarily increase the spatial smoothing.

At this point the methodology diverges depending on depth. Because substantial microseismicity is not expected to occur along the slab surface once it descends below the hanging wall mantle wedge, most observed seismicity at these depths will occur within the slab itself [e.g., Kirby *et al.*, 1996]. Thus, using seismicity above 40 km depth (the approximate location of the Mohorovičić discontinuity (Moho) in this region [DeShon *et al.*, 2006]), we identify the location of the slab interface using the *maximum seismicity method* (described below). Below 40 km depth, we use an envelope function in which we map the weighted 3-D position of the top of the seismicity (between the 80th and 90th percentile along the z' profile) to approximate the slab interface. For the region updip of the trench, the slab geometry is defined as the bathymetric seafloor surface above the sediments as obtained from both satellite- and ship-based methods [Smith and Sandwell, 1997; Ranero *et al.*, 2005].

The maximum seismicity method developed here attempts to define the fault location at depth on which the majority of microseismicity occurs within the established parabolic bounds. For each z' profile along individual grid points, a sliding window with one seventh of the total width of the profile is used to count the frequency of earthquakes along the parabola-normal profile, and the window with the most events is retained for further analysis—when two windows have equal and maximum values, the shallower one is chosen. From this maximum seismicity window, a new 3-D position is determined from the weighted average positions of the orthogonal components of the seismicity within that bin.

The weighting of events (W) within the maximum seismicity window is defined as the product of the normalized weight of the event within its catalog (W_E), and the weight of catalog relative to its along-strike position (W_C). The W_E is the inverse of the normalized component error of individual event within its catalog. Catalog quality is dependent on the network size, density, and position, as well as the catalog location method. Thus, we define W_C to represent the quality of individual catalogs as functions of their positions along-strike the MAT (varying from 0 to 2; Figure 3).

Once the new 3-D position for each grid node is determined and before generating the final surface, we apply a variable smoothness algorithm based on the spatial resolution provided by the minimum cylinder radius. The smoothness along the interface is controlled by a Gaussian-weighted average of neighboring

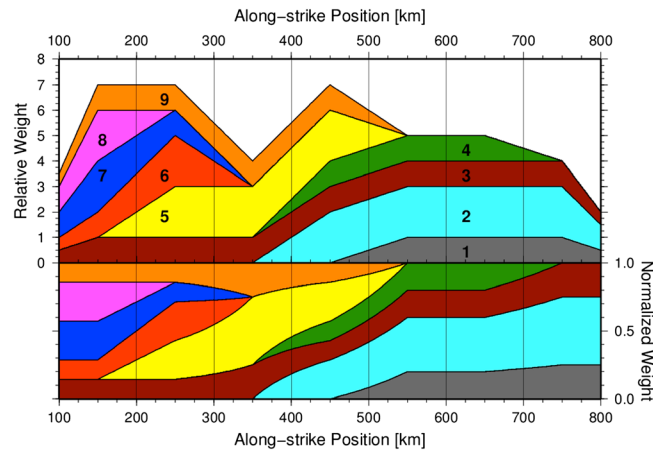


Figure 3. Representation of the (top) absolute and (bottom) normalized weighting as a function of along-strike distance. The weighting from each catalog is described as a trapezoid with maximum relative widths of 1 or 2 depending on the overall quality and location of the seismic network along-strike. Each catalog is color coded and ordered according to their representation in Figure 1. The along-strike distance corresponds to the northeast trending 100 km bins in Figure 1, with 100 and 800 km corresponding to the SE and NW most lines, respectively.

for which we describe the slab interface, the results remain extremely stable (most less than 2.5 km variability), but large errors remain in the observation of the offshore slab updip of Nicaragua and may be due to the contribution of some seismicity within the hanging wall. The lowest variability remains under the Nicoya Peninsula and offshore regions immediately to the NW and SE where dense on-land and offshore seismic networks recorded most of the seismicity.

4. Results and Discussion

For clarity, we focus much of the discussion on and around the Nicoya Peninsula, the region in which the seismogenic portion of the interface is best determined and is of most concern for our efforts to model fault behavior [Kyriakopoulos and Newman, 2014]. Across the Nicoya Peninsula we detail three downdip profiles separated each by 20 km, sampling a strong transition in subducted topography. The complete profiles spanning the model from north to south are presented in the supporting information (Figure S1).

4.1. Comparison With Other Models

The regional microseismicity is largely in agreement with the new interface model (Figures 5 and S1). We are interested in the identification of geometric features that may play a role in interseismic coupling and also contribute as asperities or barriers during the rupture phase. As expected given the algorithms we developed, above 40 km depth, the new model describes well the Nicoya component of CRSEIZE (dataset 5, yellow dots in Figure 1b) where seismicity reveals the shape variation of the interface between profiles 340 and 380. Below 40 km depth, the interface lies near the top of the seismicity, due to the change in methodology, which accounts for sub-Moho seismicity occurring primarily within the slab. We calculated the average residual depth between the interface and the seismicity to be 5.5 km at depths shallower than 40 km, increasing to 17 km below 40 km. The increase in residuals at greater depth likely reflects both changes in the method for determining the interface location and increased scatter in locating deeper earthquakes due to decreased relative network aperture to event depth. The final interface model extends from southern Costa Rica to northern Nicaragua (Figure 4) and has a length of ~700 km. The southeastern edge of the model reaches depths greater than 120 km. Because smoothing is adaptively modulated based on resolution, the new model exhibits a rougher interface at shallower depths.

We compare the final interface model with the Slab1.0 model for Central America [Hayes et al., 2012]. Figure S1 shows a series of along-dip projections across the model showing both our model and Slab1.0 with the seismic data used here. As expected, our model better describes the data, including descriptions of the

interface nodes, whose 1 sigma radius is equal to the node resolution as defined by the search radius necessary to obtain 25 nearby earthquakes (shown in Figure 4a). For regions near the edge of the model, results are only retained when more than 50% of the smoothed area is defined. The spatial resolution varies between our starting radius (5 km) and 20 km for most of the region, with the lowest values in regions where dense seismic networks exist over the interface, most prominently the seismogenic interface beneath the Nicoya Peninsula.

To evaluate the variability the model allows given our data, we perform a bootstrap analysis of the smoothed positions using 50 randomly resampled catalogs. The standard deviation of the smoothed results (Figure 4b) show that for most of the downdip environment

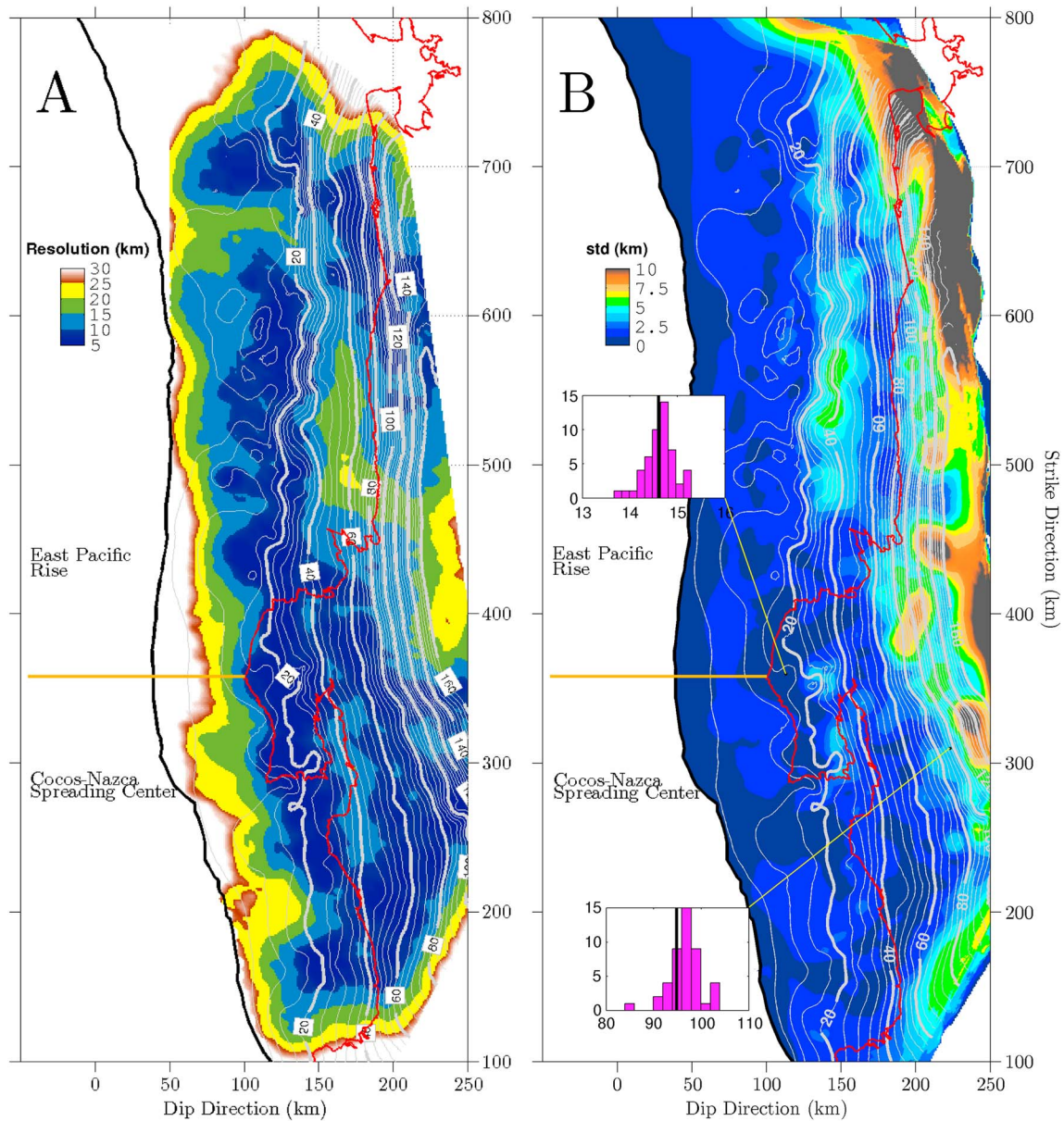


Figure 4. New 3-D slab interface model, with resolution and accuracy maps. (a) The resolution is determined to be the radius of the maximum seismicity window used for determining the slab surface (minimum fixed at 5 km). (b) The model accuracy (standard deviation) is shown from 50 randomly resampled bootstrap runs of the smoothed model interface. The x, y axes represent a local Cartesian system oriented along the approximate strike of the Middle America Trench (45° CCW from the north) and origin in longitude = -86.4° , latitude = 7° . The projected transition from East Pacific Rise (EPR) to Cocos Nazca Spreading Center (CNS) is represented with a solid yellow line. Depth (white 4 km contours), Nicaraguan and Costa Rican coastline (red line) and the Middle America Trench (thick black line) are also shown.

slab in some downdip regions not covered by Slab1.0, particularly in northern Nicaragua. The new model also shows significant variability in shape, more closely mimicking the seismicity. Along with Slab1.0, we further evaluate some of the local features we identify relative to other regional published interface models for the Nicoya region from *DeShon et al.* [2006] and *Ranero et al.* [2005], hereafter called DS06 and RN05, respectively (Figure 6). We specifically examine three cross sections (Figures 5d–5f) across the central sector of the peninsula to investigate the local-scale variability in geometric shape of the plate interface. Below Nicoya, the most visible feature is observed around $y = 350$ km (section 350, Figure 5e) indicating an abrupt change of the subduction slab geometry. This feature is coincident with a previously detected 5 km interface offset across the transition from EPR to CNS crust [*Newman et al.*, 2002] and is also apparent, though more smoothed in DS06, but not in RN05 or Slab1.0. Across this transition, the subducting crust of

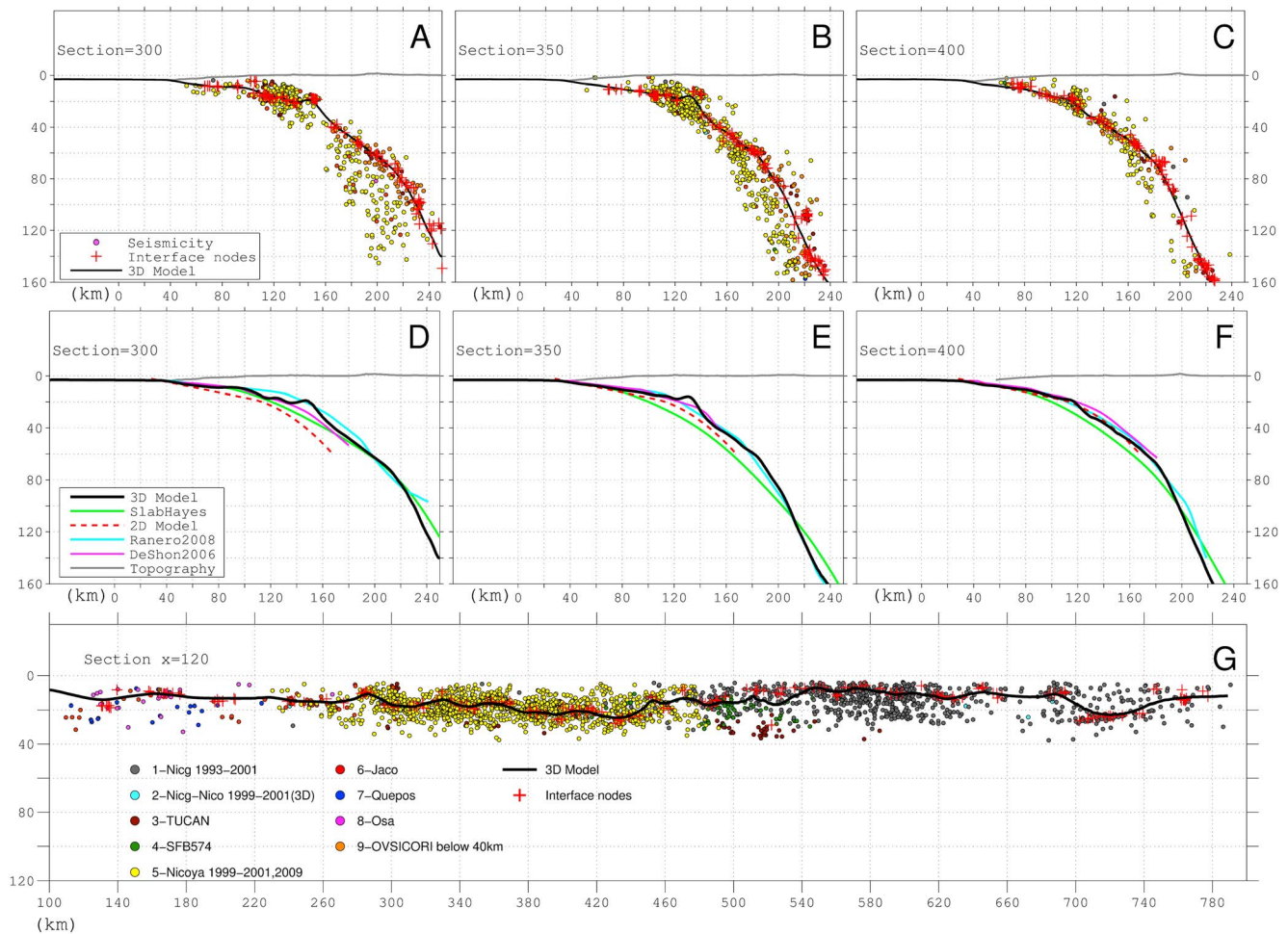


Figure 5. Model and seismicity profiles along the Nicoya Peninsula. The sections correspond to (a) northern Nicoya ($y = 400$ km), (b) central Nicoya just south of the EPR-CNS transition ($y = 350$ km), and (c) southern Nicoya ($y = 300$ km). (d-f) Model comparisons are shown for the same sections (*Ranero et al.* [2005], *DeShon et al.* [2006], *Hayes et al.* [2012], and the 2-D model from *Feng et al.* [2012]). (g) Along-strike transect for $x = 120$, corresponding to the approximate center of the megathrust. All events within 10 km of the profiles are projected onto the plane and colored according to the source data set (see legend in Figure 5g). The red crosses (in Figures 5a–5c and 5g) represent the final interface nodes before smoothing.

CNS origin to the south dips more shallowly than does the EPR crust in the north. Below Nicoya the new model is consistently shallower than Slab1.0 and represents better the local seismicity recorded primarily by the local dense Nicoya networks (Figure 1). The final 3-D model provides good agreement with various data sets. Although the DS06 and RN05 models are based on different data sets and generated using different techniques, around the central part of the Nicoya Peninsula there is relatively good agreement with the interface described in this study.

4.2. EPR-CNS Transition

The portion of the interface below the central part of the Nicoya Peninsula, specifically the seismogenic zone between about 15 and 25 km depth, is characterized by spatial variations in the geometry of the fault and resembles a subducted plateau in which the subducting CNS-1 crust remains relatively flat until about 20 km depth before descending rapidly and again matching the EPR slab to the north. Though we are uncertain of the origin, the “plateau” may be the result of relatively resistant CNS-1 subduction almost perpendicular to plate generation direction. Farther to the north *Ranero and von Huene* [2000] identify the highly effective deformation and faulting within the EPR crust that is subducting parallel to plate generation direction, possibly reactivating planes of weakness developed during formation. An alternative possibility is that a massive seamount or otherwise thickened crust along the CNS-1 crust was subducted.

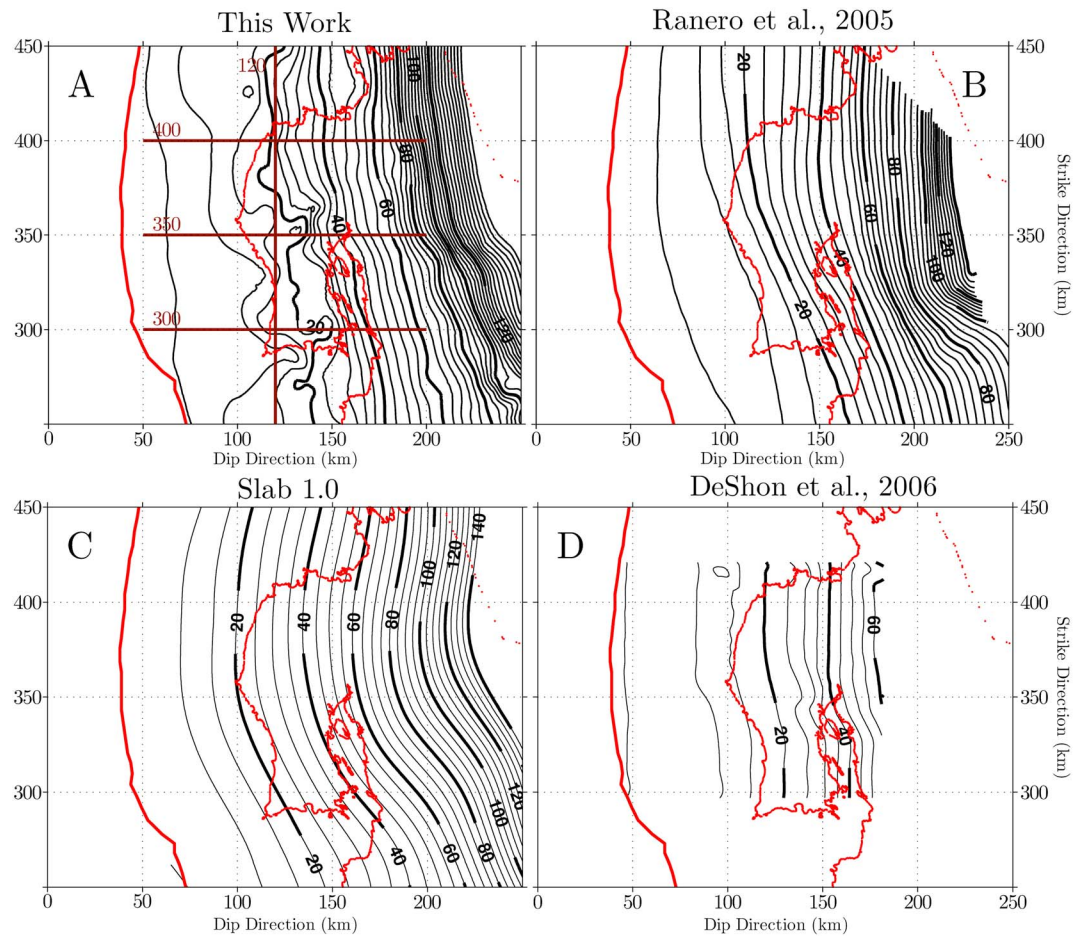


Figure 6. Comparisons of 3-D models in the Nicoya region. (a) This work is shown with the trace of the profiles shown in Figure 5. The other models are (b) RN05 from *Ranero et al.* [2005], (c) Slab1.0 from *Hayes et al.* [2012], and (d) DS06 from *DeShon et al.* [2006]. The x and y axes represent a local Cartesian system described in Figure 4. Depth contours (black thin and thick lines), the Nicoya Peninsula coastline, and MAT (red lines) are also shown.

A curious feature appearing to be a massive slump (70×140 km) exists across the margin wedge offshore most of the southern half of the Nicoya Peninsula (Figures 7 and 8). The slump corresponds to the trace of the observed CNS-1 plateau just after burial in the subduction zone assuming that there has been no substantial change in the current plate convergence direction since 1.2 Ma (Figure 7). At current plate rates, the onset of impingement of the suspected interface plateau at the trench began approximately then, with the tail of the plateau finally passing downdip of the bathymetric slump at about 400 ka. Similar and smaller scars observed across the Quepos plateau just to the south of Nicoya are traced to currently subducted seamount chains and some moderate earthquakes with complex rupture histories [*Ranero and von Huene, 2000; Bilek et al., 2003*]. While we do not know if this slump is the result of prior impingement of the interface feature we observe beneath Nicoya, its existence is strongly indicative of the recent subduction of a substantial disruptive feature.

4.3. Fisher Seamount Chain

The oceanic crust subducting along the southern most extent of the Nicoya Peninsula appears to be highly complex. When compared to the bathymetry immediately offshore, it is clear that the structures downdip line-up with the Fisher seamount chain (deflection in 16 and 20 km slab contours in Figures 7). Thus, it is our interpretation that this feature represents the subducted extension of the Fisher range. This is supported by seismic tomography performed from aftershocks of the 1990 Quepos earthquake, which found what appeared to be a large subducted seamount at about 25 km depth, possibly acting as an asperity dictating the geometry and size of the 1990 main shock [*Husen et al., 2002*]. Most recently, new

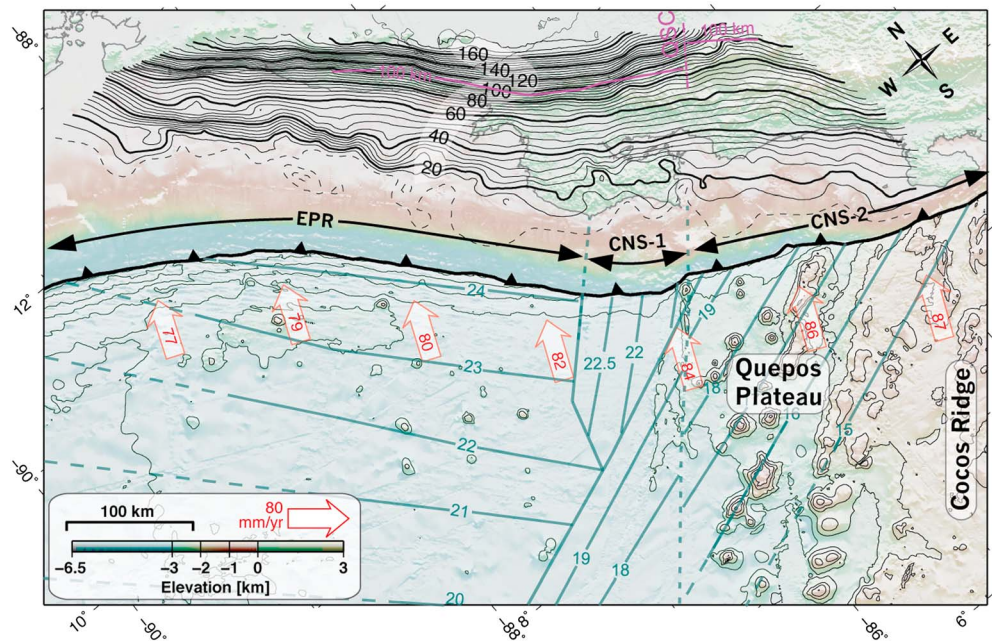


Figure 7. Regional physiography and slab model. The 4 km contoured slab surface projection is shown with the combined regional topography and bathymetry. The offshore bathymetric surface reveals the transition from a “rougher” Quepos plateau to “smoother” seafloor offshore Nicoya and Nicaragua, where Cocos Nazca Spreading Center crust (CNS-1, CNS-2) transitions to East Pacific Rise (EPR) generated crust. The solid and dashed green lines represent the approximate seafloor age (in Myr) as identified by *Barckhausen et al.* [2001]. The thick “toothed” line represents the Middle America Trench (MAT). Red velocity vectors show the Cocos Plate motion relative to the Caribbean Plate [*DeMets et al.*, 2010]. Also shown is the magenta 100 km contour and Quesada Sharp Contortion (QSC) from *Protti et al.* [1994]. The 12 km subducted contour farthest offshore (thin dashed line) is seaward of the seismic networks and remains poorly resolved.

analysis of satellite gravity by *Sandwell et al.* [2014] show a strong positive free-air gravity anomaly along the trend of the Fisher seamount chain approximately halfway between the trench and the southeastern tip of the Nicoya Peninsula, supplying further evidence for the downdip extension of the Fisher seamount chain (Figure 8). Interface topography has long been recognized to play a controlling role in the slip behavior along megathrust environment [e.g., *Kanamori*, 1986]. In Costa Rica magnitude 7 events have been associated with the mechanical heterogeneities produced by subducted seamounts [*Bilek et al.*, 2003].

4.4. The Quepos Plateau

A dominant feature of the oceanic plate in the region is a transition from the apparently smooth seafloor offshore Nicaragua and Nicoya to a substantially rougher and more elevated bathymetry along the Quepos plateau (Figure 7). In particular, a seamount chain (standing approximately 2.5 km high) located halfway between the Nicoya and Osa Peninsulas dominates the plateau and corresponds to a large erosional indentation in the margin wedge, similar in size to the slump observed offshore southern Nicoya [*von Huene et al.*, 2000; *Ranero and von Huene*, 2000]. This and other grooves associated with regional seamounts along the plateau were previously identified as path markers for underthrusting seamounts beneath the continental slope [*Ranero and von Huene*, 2000].

4.5. The General Role of Interface Topography

The debate over whether the seamounts act primarily as seismic asperities or are largely aseismic is still open, and nowadays there is evidence to support both theses. For example, regions of elevated topography may be sites which expose otherwise underlying lithologies including chalk, which are characterized by frictionally unstable behavior [*Marone*, 1998]. This contrasts most environments where weak hemipelagic sediments including clays, are dominant along the interface. In this scenario the local topographic highs act to localize the strain, acting as earthquake asperities, while surrounding weak sediments favor rupture propagation [*Ikari et al.*, 2013]. Recently, *Wang and Bilek* [2011] suggested that subducted topography might allow for

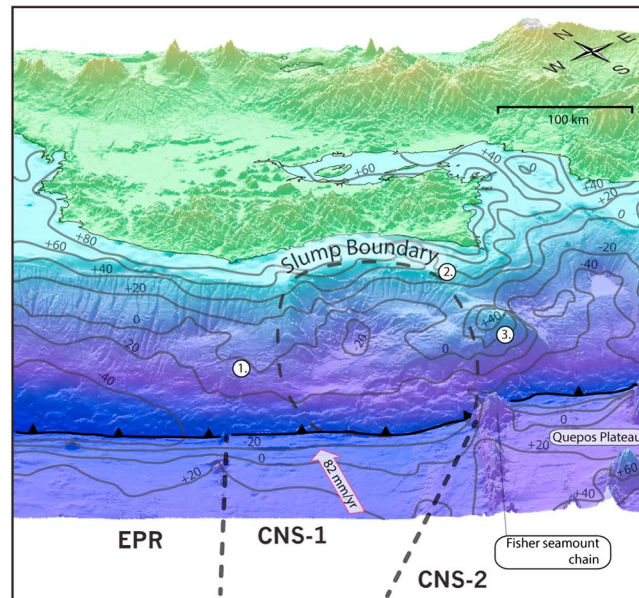


Figure 8. Gravity [Sandwell *et al.*, 2014] and physiographic makeup of the area around the Nicoya Peninsula [Ryan *et al.*, 2009]. Free-air gravity (gray contours reported in milligals) and the 30° dipping perspective of the bathymetry and topography (approximately -4 km to $+1$ km elevation). This view highlights some subducted features due to the differential makeup of the incoming oceanic plate, consisting of East Pacific Rise (EPR), and Cocos-Nazca Spreading Center Crust before (CNS-1) and after (CNS-2) a change in plate orientation, relative to the overriding shelf. Three features are dominant (enumerated in plot). 1.: A positive gravity anomaly exists along the CNS-1 side of the EPR-CNS transition approximately midway up the slope. 2.: To the south, a large physiographic and gravity anomaly is likely a large slump that extends from near the shore all the way down to the trench (bounded by curved dashed line), possibly due to the subduction of a substantial topographic high. 3.: Farther to the south, the subduction of the Fisher seamount appears to continue into the megathrust with a large positive topographic and gravity high approximately 40 km inland of the trench. These three subducted features appear to continue further downdip and are apparent in our new slab geometry (Figure 7).

maximum seismicity method in combination with a limiting envelope function for the interface below the Moho. The new interface is characterized by both lateral and down section heterogeneities, the correspond with seafloor features (seamounts and slumps), and regions of geodetic locking and slip (models of Feng *et al.* [2012], Yue *et al.* [2013], and Protti *et al.* [2014]). The marked geometric shape variations observed between 15 and 25 km beneath the Nicoya Peninsula are coincident with a transition in oceanic crust between that generated at the East Pacific Rise and the Cocos-Nazca Spreading Center and correspond to a large apparent slump offshore the peninsula. An additional smaller peak off of southern Nicoya corresponds with the downdip extension of the current Fisher seamount chain. The new model captures local features of the slab topography that we cannot see in previous models, especially around Nicoya Peninsula. While the three-dimensional model was developed primarily for geodetic inversions of interface locking and earthquake slip, it is likely of value for a number of geodynamic and regional structural models.

References

- Arroyo, I. G., S. Husen, E. R. Flueh, J. Gossler, E. Kissling, and G. E. Alvarado (2009), Three-dimensional P -wave velocity structure on the shallow part of the Central Costa Rican Pacific margin from local earthquake tomography using off- and onshore networks, *Geophys. J. Int.*, *179*, 827–849, doi:10.1111/j.1365-246X.2009.04342.x.
- Barckhausen, U., C. Ranero, R. von Huene, S. Cande, and H. Roeser (2001), Revised tectonic boundaries in the Cocos Plate off Costa Rica: Implications for the segmentation of the convergent margin and for plate tectonic models, *J. Geophys. Res.*, *106*(B9), 19,207–19,220, doi:10.1029/2001JB000238.

aseismic sliding between the two plates during the interseismic period, because of the release of high-pressure fluids that reduce the effective normal stress, and thus would not act as an asperity for large earthquakes. Similarly, seismic surveys from the southern segment of the Japan Trench showed that a subducted seamount might produce weakly coupled zones along the plate interface, modulating the area of rupture [Mochizuki *et al.*, 2008]. Additionally, using dynamic rupture models, Yang *et al.* [2013] showed that if an earthquake nucleates very near a seamount, the structure might actually act as a barrier, inhibiting rupture. Nonetheless, it is clear that geometric complexities act as mechanical regulators during both the interseismic and coseismic phases, producing a combined geometry-lithology effect. It is logical that a better characterization of the fault interface is a necessary initial step toward developing more realistic representations of seismogenic zone behavior through the seismic cycle.

5. Conclusions

Using data from a combined seismic catalog of $\sim 30,000$ events, we developed a high-resolution subduction interface model beneath the Nicaraguan and Costa Rica segments of Middle America Trench using the newly defined maxi-

Acknowledgments

Support for C.K. was provided through NSF-0847382 to AVN (Postdoc Advisor). The figures were generated using GMT [Wessel *et al.*, 2013] and M_Map (<http://www.eos.ubc.ca/~rich/map.html>). High-resolution oceanic bathymetry and on-land topography are compiled through the Global Multi-Resolution Topography project [Ryan *et al.*, 2009] and included substantial local ship-based bathymetry [Ranero and von Huene, 2000]. Composite earthquake catalogs and the final MAT slab models are available at <http://nicoya.eas.gatech.edu>.

- Bilek, S. L., S. Y. Schwartz, and H. R. DeShon (2003), Control of seafloor roughness on earthquake rupture behavior, *Geology*, *31*(5), 455–458, doi:10.1130/0091-7613(2003)031.
- DeMets, C., R. G. Gordon, and D. F. Argus (2010), Geologically current plate motions, *Geophys. J. Int.*, *181*, 1–80, doi:10.1111/j.1365-246X.2009.04491.x.
- DeShon, H. R., S. Y. Schwartz, S. L. Bilek, L. M. Dorman, V. Gonzalez, J. M. Protti, E. R. Flueh, and T. H. Dixon (2003), Seismogenic zone structure of the southern Middle America Trench, Costa Rica, *J. Geophys. Res.*, *108*(B10), 2491, doi:10.1029/2002JB002294.
- DeShon, H. R., S. Y. Schwartz, A. V. Newman, V. Gonzalez, J. M. Protti, L. M. Dorman, T. Dixon, D. E. Sampson, and E. R. Flueh (2006), Seismogenic zone structure beneath the Nicoya Peninsula, Costa Rica, from three-dimensional local earthquake P- and S-wave tomography, *Geophys. J. Int.*, *164*, 109–124, doi:10.1111/j.1365-246X.2005.02809.x.
- Dinc, A. N., I. Koulakov, M. Thorwart, W. Rabbel, E. R. Flueh, I. Arroyo, W. Taylor, and G. Alvarado (2010), Local earthquake tomography of central Costa Rica: Transition from seamount to ridge subduction, *Geophys. J. Int.*, *183*, 286–302, doi:10.1111/j.1365-246X.2010.04717.x.
- Duan, B., and D. D. Oglesby (2005), Multicycle dynamics of nonplanar strike-slip faults, *J. Geophys. Res.*, *110*, B03304, doi:10.1029/2004JB003298.
- Eberhart-Phillips, D. (1990), Three-dimensional P and S velocity structure in the Coalinga region, California, *J. Geophys. Res.*, *95*, 15,343–15,363, doi:10.1029/JB095iB10p15343.
- Evans, J. R., D. Eberhart-Phillips, and C. H. Thurber (1994), User's manual for SIMULP512 for imaging V_p and V_p/V_s : A derivative of the "Thurber" tomographic inversion SIMUL3 for local earthquakes and explosions, *U.S. Geol. Surv. Open File Rep.*, 94-431.
- Feng, L., A. V. Newman, J. M. Protti, V. González, Y. Jiang, and T. H. Dixon (2012), Active deformation near the Nicoya Peninsula, northwestern Costa Rica, between 1996 and 2010: Interseismic megathrust coupling, *J. Geophys. Res.*, *117*, B06407, doi:10.1029/2012JB009230.
- Gudmundsson, O., and M. Sambridge (1998), A regionalized upper mantle (RUM) seismic model, *J. Geophys. Res.*, *103*, 7121–7136, doi:10.1029/97JB02488.
- Harris, R. N., G. Spinelli, C. R. Ranero, I. Grevemeyer, H. Villinger, and U. Barckhausen (2010), Thermal regime of the Costa Rican convergent margin: 2. Thermal models of the shallow Middle America subduction zone offshore Costa Rica, *Geochem. Geophys. Geosyst.*, *11*, Q12529, doi:10.1029/2010GC003273.
- Hayes, G. P., D. J. Wald, and R. L. Johnson (2012), Slab1.0: A three-dimensional model of global subduction zone geometries, *J. Geophys. Res.*, *117*, B01302, doi:10.1029/2011JB008524.
- Husen, S., E. Kissling, and R. Quintero (2002), Tomographic evidence for a subducted seamount beneath the Gulf of Nicoya, Costa Rica: The cause of the 1990 $M_w = 7.0$ Gulf of Nicoya earthquake, *Geophys. Res. Lett.*, *29*(8), 1238, doi:10.1029/2001GL014045.
- Ikari, M. J., A. R. Niemeijer, C. J. Spiers, A. J. Kopf, and D. M. Saffer (2013), Experimental evidence linking slip instability with seafloor lithology and topography at the Costa Rica convergent margin, *Geology*, *41*, 891–894, doi:10.1130/G33956.1.
- Kanamori, H. (1986), Rupture process of Subduction-zone earthquakes, *Annu. Rev. Earth Planet. Sci.*, *14*, 293–322.
- Kikuchi, M., and H. Kanamori (1995), The Shikotan Earthquake of October 4, 1994: Lithospheric earthquake, *Geophys. Res. Lett.*, *22*(9), 1025–1028, doi:10.1029/95GL00883.
- Kirby, S., R. E. Engdahl, and R. Denlinger (1996), Intermediate-depth intraslab earthquakes and arc volcanism as physical expressions of crustal and uppermost mantle metamorphism in subducting slabs, in *Subduction Top to Bottom*, *Geophys. Monogr. Ser.*, vol. 96, edited by G. E. Bebout et al., pp. 195–214, AGU, Washington, D. C., doi:10.1029/GM096p0195.
- Kyriakopoulos, C., and A. V. Newman (2014), Topographic regulators of the seismic cycle along the subduction megathrust, Abstract T51A-4586 presented at the 2014 Fall Meeting, AGU, San Francisco, Calif., 15–19 Dec.
- Marone, C. (1998), Laboratory-derived friction laws and their application to seismic faulting, *Annu. Rev. Earth Planet. Sci.*, *26*, 643–696, doi:10.1146/annurev.earth.26.1.643.
- Mochizuki, K., T. Yamada, M. Shinohara, Y. Yamanaka, and T. Kanazawa (2008), Weak interplate coupling by seamounts and repeating $M \sim 7$ earthquakes, *Science*, *321*(5893), 1194–1197, doi:10.1126/science.1160250.
- Moore-Driskell, M., H. R. DeShon, W. Rabbel, M. Thorwart, Y. Dzierma, and I. G. Arroyo (2013), Integration of arrival-time datasets for consistent quality control: A case study of amphibious experiments along the Middle America Trench, *Bull. Seismol. Soc. Am.*, *103*(5), 2752–2766, doi:10.1785/01201202274.
- Newman, A. V., S. Y. Schwartz, V. González, H. R. DeShon, J. M. Protti, and L. M. Dorman (2002), Along-strike variability in the seismogenic zone below Nicoya Peninsula, Costa Rica, *Geophys. Res. Lett.*, *29*(20), 1977, doi:10.1029/2002GL015409.
- Pacheco, J., and L. Sykes (1992), Seismic moment catalog for large shallow earthquakes from 1900 to 1989, *Bull. Seismol. Soc. Am.*, *82*, 1306–1349.
- Protti, M., F. Güendel, and K. McNally (1994), The geometry of the Wadati-Benioff zone under southern Central America and its tectonic significance: Results from a high-resolution local seismographic network, *Phys. Earth Planet. Inter.*, *84*, 271–287, doi:10.1016/0031-9201(94)90046-9.
- Protti, M., V. González, A. V. Newman, T. H. Dixon, S. Y. Schwartz, J. S. Marshall, L. Feng, J. I. Walter, R. Malservisi, and S. E. Owen (2014), Nicoya earthquake rupture anticipated by geodetic measurement of the locked plate interface, *Nat. Geosci.*, *7*, 117–121, doi:10.1038/ngeo2038.
- Ranero, C. R., and R. von Huene (2000), Subduction erosion along the Middle America convergent margin, *Nature*, *404*, 748–752, doi:10.1038/35008046.
- Ranero, C. R., A. Villaenor, J. Phipps Morgan, and W. Weinrebe (2005), Relationship between bend-faulting at trenches and intermediate-depth seismicity, *Geochem. Geophys. Geosyst.*, *6*, Q12002, doi:10.1029/2005GC000997.
- Ryan, W. B. F., et al. (2009), Global multi-resolution topography synthesis, *Geochem. Geophys. Geosyst.*, *10*, Q03014, doi:10.1029/2008GC002332.
- Sandwell, D. T., R. D. Müller, W. H. F. Smith, E. Garcia, and R. Francis (2014), New global marine gravity model from CryoSat-2 and Jason-1 reveals buried tectonic structure, *Science*, *346*, 65–67, doi:10.1126/science.1258213.
- Smith, W. H. F., and D. T. Sandwell (1997), Global seafloor topography from satellite altimetry and ship depth soundings, *Science*, *277*, 1957–1962.
- Syracuse, E. M., and G. A. Abers (2006), Global compilation of variations in slab depth beneath arc volcanoes and implications, *Geochem. Geophys. Geosyst.*, *7*, Q05017, doi:10.1029/2005GC001045.
- Syracuse, E. M., G. A. Abers, K. Fischer, L. MacKenzie, C. Rychert, M. Protti, V. Gonzalez, and W. Strauch (2008), Seismic tomography and earthquake locations in the Nicaraguan and Costa Rican upper mantle, *Geochem. Geophys. Geosyst.*, *9*, Q07508, doi:10.1029/2008GC001963.
- Thurber, C. H. (1983), Earthquake locations and three-dimensional crustal structure in the Coyote Lake area, central California, *J. Geophys. Res.*, *88*, 8226–8236, doi:10.1029/JB088iB10p08226.
- Thurber, C. H. (1993), Local earthquake tomography: Velocities and V_p/V_s -theory, in *Seismic Tomography: Theory and Practice*, edited by H. M. Iyer and K. Hirahara, pp. 563–583, Chapman and Hall, London.

- von Huene, R., C. R. Ranero, W. Weinrebe, and K. Hinz (2000), Quaternary convergent margin tectonics of Costa Rica, segmentation of the Cocos Plate, and Central American volcanism, *Tectonics*, *19*, 314–334, doi:10.1029/1999TC001143.
- Wang, K., and S. L. Bilek (2011), Do subducting seamounts generate or stop large earthquakes?, *Geology*, *39*, 819–822, doi:10.1130/G31856.1.
- Wessel, P., W. H. F. Smith, R. Scharroo, J. F. Luis, and F. Wobbe (2013), Generic Mapping Tools: Improved version released, *Eos Trans. AGU*, *94*, 409–410, doi:10.1002/2013EO450001.
- Yang, H., Y. Liu, and J. Lin (2013), Geometrical effects of a subducted seamount on stopping megathrust ruptures, *Geophys. Res. Lett.*, *40*, 1–6, doi:10.1002/grl.50509.
- Yue, H., T. Lay, S. Y. Schwartz, L. Rivera, M. Protti, T. H. Dixon, S. Owen, and A. V. Newman (2013), The 5 September 2012 Nicoya, Costa Rica M_w 7.6 earthquake rupture process from joint inversion of high-rate GPS, strong-motion, and teleseismic P wave data and its relationship to adjacent plate boundary interface properties, *J. Geophys. Res. Solid Earth*, *118*, 5453–5466, doi:10.1002/jgrb.50379.

Supplementary Informations (SI) - Figure captions (S1, S2) for "A new seismically constrained subduction interface model for Central America"

Kyriakopoulos, C.¹, A.V. Newman¹, A. M. Thomas^{1,2,3}, M. Moore-Driskell⁴, G. T. Farmer¹

¹Georgia Institute of Technology, School of Earth and Atmospheric Sciences
311 Ferst Drive, Ford ES&T building 30332-0340, Atlanta, Georgia, USA

²Stanford University, Department of Geophysics
397 Panama Mall, 94305, Stanford, California, USA

³University of Oregon, Department of Geological Sciences
1272 University of Oregon, Eugene, Oregon, 97403-1272, USA

⁴University of North Alabama, Department of Physics and Earth Science, Florence, AL 35632,
UNA Box 5065

Corresponding author: christos@ucr.edu

Figure S1. Cross-Sections (50 km step) South to North (100-750). See **Figure S2** for profile section surface projection. For symbols see legend in last panel.

Figure S2. Down section profiles (50 km step). This figure shows the geographic position of cross-sections relative to the new interface model. The MAT trench and Nicaragua-Costa Rica coastline are represented with a thick and thin red line respectively.

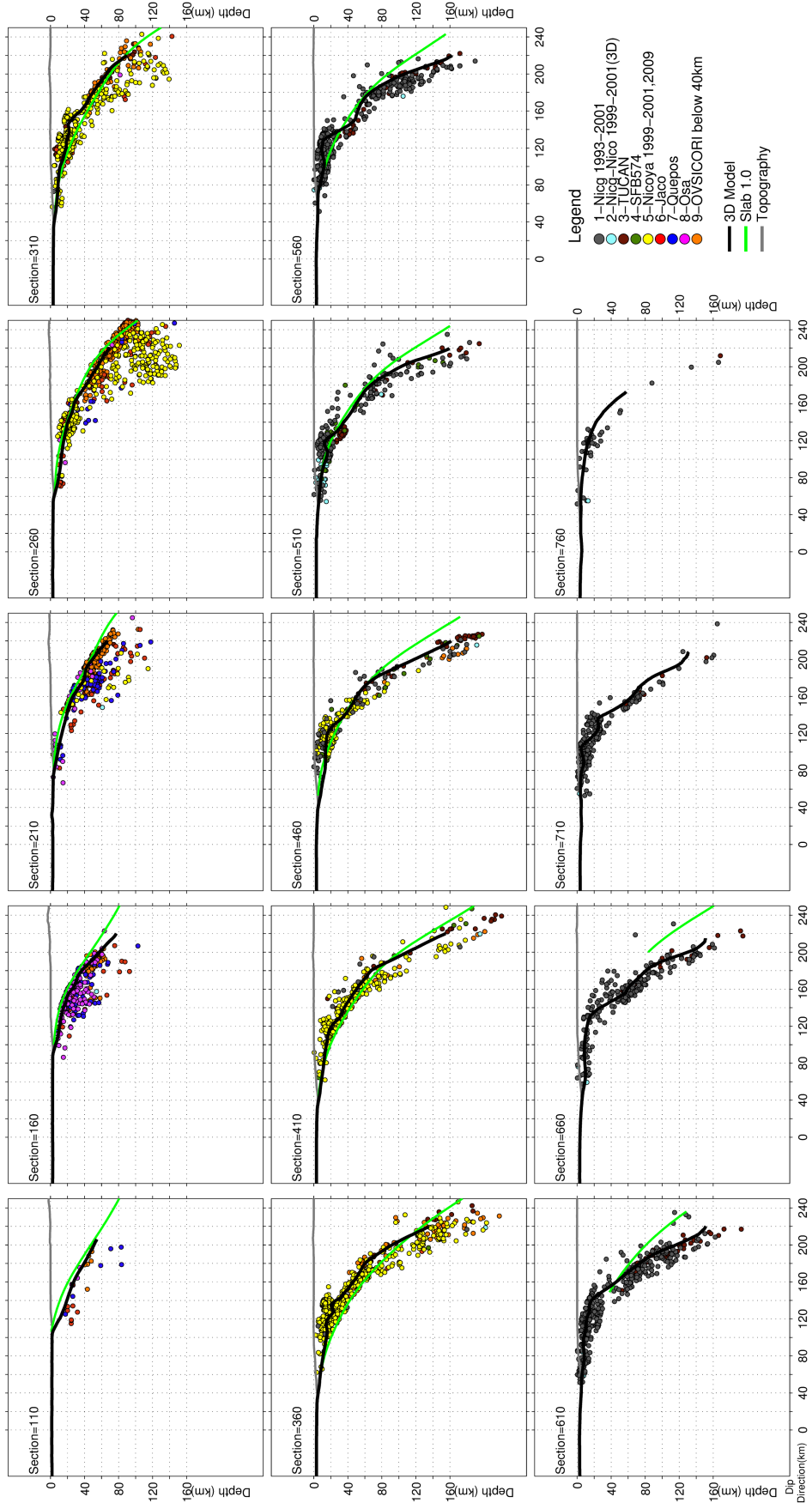


Figure S1.

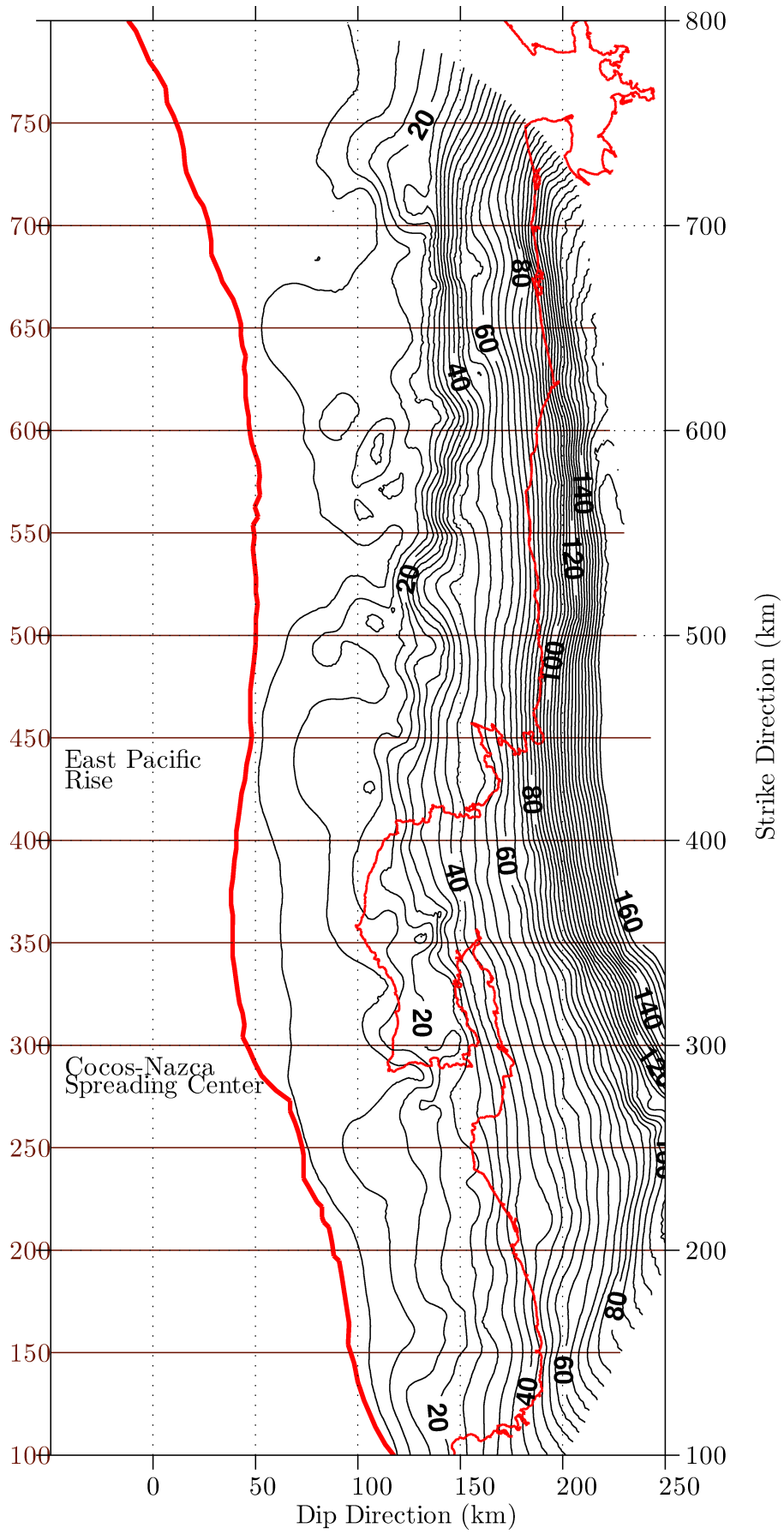


Figure S2.